JOURNAL OF GUIDANCE, CONTROL, AND DYNAMICS
Vol. 28, No. 2, March–April 2005

Dynamic Behavior of an Orbiter Around Europa

Martín Lara*
Real Observatorio de la Armada, 11110 San Fernando, Spain
and
Juan F. San Juan†
Universidad de La Rioja, 26004 Logroño, Spain

The dynamics of an orbiter close to a planetary satellite are known to be unstable from a wide range of inclinations encompassing polar orbits. Taking the Jupiter–Europa system as our model, we use numerically determined periodic orbits to investigate the stability of motion over three-dimensional space for this problem. We have found that the change in stability is produced by a bifurcation in phase space. At a certain critical inclination, almost circular periodic orbits change their stability character to instability and new families of (stable) elliptic orbits appear.

Nomenclature

a	=	semimajor axis (one of the six orbital elements)
b	=	stability index, $\lambda + \lambda^{-1}$
C_1	=	another form of the z component of the angular momentum
C_2	=	another form of the Jacobi integral
d	=	distance between the centers of mass of the planet and the satellite
e	=	eccentricity (one of the six orbital elements)
f	=	true anomaly
$\mathcal{G}_z$	=	z component of the angular momentum
g	=	argument of the pericenter (one of the six orbital elements)
h	=	equinoctial element, $e \sin g$
I	=	inclination (one of the six orbital elements)
$\boldsymbol{i}, \boldsymbol{j}, \boldsymbol{k}$	=	unit vectors, rotating frame with origin at the center of mass of the satellite
$\mathcal{J}$	=	Jacobi integral
J_2	=	satellite's oblateness coefficient
k	=	equinoctial element, $e \cos g$
n	=	mean motion, average angular velocity of the orbiter
R	=	disturbing function, third-body effect plus nonsphericity perturbation
$\boldsymbol{R}$	=	position vector of the orbiter with respect to the center of mass of the planet–satellite system
$\boldsymbol{R}_1$	=	position vector of the orbiter with respect to the center of mass of the planet
$\boldsymbol{r}$	=	position vector of the orbiter with respect to the center of mass of the satellite
T	=	nodal period, time between two upward passages of the orbiter through the equatorial plane of the satellite
t	=	time
V	=	potential energy of the orbiter produced by the gravity of the satellite
x, y, z	=	rectangular coordinates of the orbiter in the rotating frame
α	=	scaling parameter, the equatorial radius of the satellite
Γ	=	Jacobi constant
γ	=	another form of the stability parameter
ϵ	=	stability parameter
λ	=	eigenvalue of the monodromy matrix of a periodic orbit
μ	=	gravitational parameter, the gravitational constant times the mass of the body
$\boldsymbol{\rho}$	=	position vector of the satellite with respect to the center of mass of the system
Ω	=	longitude of ascending node (one of the six orbital elements)
$\boldsymbol{\omega}$	=	angular velocity of the rotating frame

Superscripts

$\dot{}$, $\ddot{}$	=	differentiation in the rotating frame

Introduction

THE main motivation of this work is the recent general interest in exploring Europa. NASA's Galileo spacecraft found evidence that Jupiter's moon Europa appears to have melted water relatively close to the surface. Water is an ingredient essential for life, and a recent National Research Council report[1] ranked a Europa orbiter mission as a top priority for a "flagship" solar system mission in the next decade.

The stability of orbital dynamics around a planetary satellite is studied in Ref. 2, where low-altitude, almost-circular orbits are shown to suffer from dynamic instability in a wide range of inclinations centered around polar orbits. The exponential growth in the eccentricities of unstable orbits, leading to impact,[3] is predicted in Ref. 2 by means of an analytic theory for the secular motion of an orbiter close to the planetary satellite. This theory takes into account the planetary satellite's oblateness and uses Hill's approximation to the three-body problem[4] to consider the tidal force of the planet.

In this work we restrict our study to the Jupiter–Europa case and take a different approach. Because the dynamic model[2] is formally equivalent to the dynamics of a satellite under the gravity field of a nonsymmetrical rotating body, we can proceed as in Refs. 5 and 6, where numerically determined periodic orbits are used to explore the stability of motion over three-dimensional space around nonsymmetrical rotating bodies. Once a periodic orbit is computed, the stability of the orbit can also be computed, which helps to describe the character of the phase space in the vicinity of the orbit.[7]

Families of three-dimensional periodic orbits are known to bifurcate from planar, resonant periodic orbits—orbits whose mean motion is commensurate with the rotation rate of the attracting body. The problem we are dealing with is conservative when formulated in a rotating frame and, therefore, accepts the Jacobian constant as integral of motion. Thus, we proceed as follows. First, we compute the family of almost-circular, retrograde, periodic orbits that lie on

Presented as Paper AAS 03-233 at the AAS/AIAA Space Flight Mechanics Meeting, Ponce, PR, 9–13 January 2003; received 8 October 2003; revision received 26 February 2004; accepted for publication 27 February 2004.

*Commander, Ephemeris Department; mlara@roa.es.
†Assistant Professor, Department of Matemáticas y Computación.

the equatorial (x, y) plane of the planetary satellite for variations of the Jacobian constant. Then we compute the families of almost-circular, three-dimensional, periodic orbits that bifurcate out of the plane at different resonances.

The bifurcated families of almost-circular, three-dimensional, periodic orbits evolve from retrograde to direct motion through the 180 deg of inclination. Near-circular, periodic orbits change their stability character at certain critical inclinations. Thus, for the computed families, we find large areas of instability (between 85 and 95 deg wide) centered around polar orbits. The numerical analysis carried out here shows strong differences with respect to similar analyses of the motion around asteroids. The dynamic environment of an asteroid can be highly chaotic and instability is mostly related with low-inclination direct orbits[6] (see also Ref. 8 and the references therein).

The change in the stability character of three-dimensional periodic orbits is related to qualitative changes in phase space produced by bifurcations where new families of periodic orbits appear.[9] We found that two new families of periodic orbits appear at the inclinations where the almost-circular periodic orbits change their stability character. The orbits of these new families are stable, elliptic orbits with arguments of the pericenter at 90 and 270 deg, respectively. The main effect produced by variations of the Jacobian constant is then a variation in eccentricity. Of course, most of these elliptic orbits are collision orbits—orbits producing the impact of the orbiter on the surface of the planetary satellite—because the validity of the dynamic model we used is restricted to orbits close to the planetary satellite.

The qualitative dynamics of Hill's problem can be described in terms of secular variation of orbital elements. Regardless of the motion of the nodes, we find a sufficient number of integrals to reduce the system to one degree of freedom. Then contour plots can be used to display the solutions on the plane of eccentricity vs the argument of the pericenter without having to integrate the equations of motion.[10] The nonsphericity of the central body produces significant qualitative changes in the dynamics of Hill's problem. Thus, besides the solutions obtained in Ref. 10, we found new eccentric orbits with fixed pericenter at 0 and 180 deg. Moreover, we can relate all the equilibrium solutions of the double averaged problem to periodic orbits of the original (nonaveraged) problem.

We constrained our study to the Jupiter–Europa case, but by using canonical units for our computations we removed all the parameters except the oblateness coefficient. Therefore, the results of this paper are of a more general application. To check the influence of the oblateness of the planetary satellite in systems of similar characteristics, we compute several families of periodic orbits for variations of the oblateness coefficient. As predicted in Ref. 2, the main effect produced by larger values of the oblateness coefficient is a reduction of the instability area, and there is a critical value of the oblateness coefficient for which polar orbits become stable and the instability area splits into two narrow areas of unstable motion.

To summarize our contributions: 1) By computing periodic orbit families we determine stability regions in three-dimensional space for orbital motion around oblate planetary satellites and, more specifically, around Europa. We found that the change in the stability of almost-circular orbits is produced by bifurcations of new families of stable, elliptic orbits. 2) We proved that Hill's problem perturbed by the oblateness of the planetary satellite is integrable after a double averaging. Furthermore, we find complete agreement between the secular motion dynamics and the dynamics of the original (nonaveraged) problem.

Dynamic Model

We study the motion of an orbiter O around a natural satellite S of a planet P. Because we assume that the orbiter does not influence the motion of P and S, we can use a particular case of the three-body problem. We further assume that the satellite and the planet revolve in circular orbits around their mutual center of mass with angular velocity $\boldsymbol{\omega}$, and that the distance $d = PS$ between the centers of mass of the planet and the satellite is long enough to consider P a mass point.

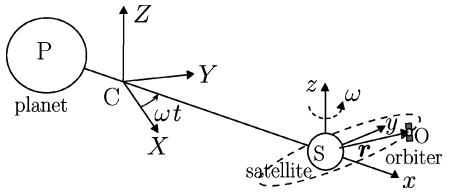

Fig. 1 Geometry of Hill's model.

We study the motion of the orbiter relative to the satellite, and we choose a rotating frame of reference with origin at the center of mass of the satellite and defined by unit vectors $(\boldsymbol{i}, \boldsymbol{j}, \boldsymbol{k})$. The x axis is in the direction of PS, the z axis is in the direction of $\boldsymbol{\omega}$, and the y axis completes a direct reference frame. We also consider an inertial frame with origin at the center of mass of the system, C. Furthermore, we assume that the equator of the satellite coincides with its orbital plane. Figure 1 describes the geometry of the motion.

Let $\boldsymbol{SO} = \boldsymbol{r} = x\boldsymbol{i} + y\boldsymbol{j} + z\boldsymbol{k}$ be the position vector of the orbiter in the rotating frame, and $\boldsymbol{CS} = \boldsymbol{\rho}$. Then $\boldsymbol{R} = \boldsymbol{\rho} + \boldsymbol{r}$ is the position vector of the orbiter in the inertial frame.

By means of the derivative in the rotating frame, where $\boldsymbol{\rho}$ is a constant vector,

$$\frac{\mathrm{d}^2\boldsymbol{R}}{\mathrm{d}t^2} = \ddot{\boldsymbol{r}} + 2\boldsymbol{\omega} \times \dot{\boldsymbol{r}} + \boldsymbol{\omega} \times (\boldsymbol{\omega} \times \boldsymbol{r}) - \omega^2\boldsymbol{\rho} \tag{1}$$

where $\mathrm{d}/\mathrm{d}t$ is the absolute derivative and dots represent differentiation in the rotating frame.

On the other hand, from Newton's gravitational law, the acceleration of the orbiter in the inertial frame is

$$\frac{\mathrm{d}^2\boldsymbol{R}}{\mathrm{d}t^2} = -\frac{\mu_p}{R_1^3}\boldsymbol{R}_1 - \boldsymbol{\nabla}_r V \tag{2}$$

where $R_1 = PO$, μ_p is the gravitational parameter of the planet (the product of the gravitational constant and the mass of the planet), and $V(\boldsymbol{r})$ is the potential energy of the orbiter produced by the gravity of the satellite.

From Eqs. (1) and (2) we have

$$\ddot{\boldsymbol{r}} + 2\boldsymbol{\omega} \times \dot{\boldsymbol{r}} + \boldsymbol{\omega} \times (\boldsymbol{\omega} \times \boldsymbol{r}) + \boldsymbol{\nabla}_r V = \omega^2\boldsymbol{\rho} - \left(\mu_p \big/ R_1^3\right)\boldsymbol{R_1} \tag{3}$$

In the inertial frame, the satellite moves under the acceleration produced by the planet's gravitation:

$$\omega^2\rho = \mu_p \big/ d^2 \tag{4}$$

Then, working at first order of r/d,

$$\frac{\mu_p}{R_1^3}\boldsymbol{R_1} = \omega^2\rho\frac{\boldsymbol{R_1}/d}{(R_1/d)^3} = \omega^2\rho\left[\left(1 - 2\frac{x}{d}\right)\boldsymbol{i} + \frac{y}{d}\boldsymbol{j} + \frac{z}{d}\boldsymbol{k}\right] \tag{5}$$

where

$$\boldsymbol{R}_1/d = (\boldsymbol{d} + \boldsymbol{r})/d = (1 + x/d)\boldsymbol{i} + (y/d)\boldsymbol{j} + (z/d)\boldsymbol{k} \tag{6}$$

$$(d/R_1)^3 = 1 - 3(x/d) + \mathcal{O}(r/d)^2 \tag{7}$$

From the definition of the center of mass,

$$d/\rho = 1 + M_S/M_P \tag{8}$$

where M is the mass. Further assuming that M_S/M_P is of higher order, and taking into account that

$$\boldsymbol{\omega} \times (\boldsymbol{\omega} \times \boldsymbol{r}) = -\omega^2(x\boldsymbol{i} + y\boldsymbol{j}) \tag{9}$$

we can write Eq. (3) as

$$\ddot{\boldsymbol{r}} + 2\boldsymbol{\omega} \times \dot{\boldsymbol{r}} = \omega^2(3x\boldsymbol{i} - z\boldsymbol{k}) - \boldsymbol{\nabla}_r V \tag{10}$$

The dot product of Eq. (10) and $\dot{\boldsymbol{r}}$ can be integrated to obtain the Jacobi integral:

$$\mathcal{J} = \tfrac{1}{2}(\dot{x}^2 + \dot{y}^2 + \dot{z}^2) + \tfrac{1}{2}\omega^2(z^2 - 3x^2) + V \tag{11}$$

where constant $\mathcal{J} = -\Gamma/2$. Equations (10) and (11) are classical Hill equations. (The derivation of those equations can be found in specialized books.[11,12]) We made the same assumptions to these as Hill.

Up to here we used the rule of derivation in a rotating frame. But, considering that $\mathrm{d}\boldsymbol{r}/\mathrm{d}t$ is the absolute derivative of $\boldsymbol{r}$, we note that Eq. (11) can be written as

$$\mathcal{J} = \frac{1}{2}\frac{\mathrm{d}\boldsymbol{r}}{\mathrm{d}t}\cdot\frac{\mathrm{d}\boldsymbol{r}}{\mathrm{d}t} - \frac{\mu}{r} - \boldsymbol{\omega}\cdot\boldsymbol{r}\times\frac{\mathrm{d}\boldsymbol{r}}{\mathrm{d}t} - R \tag{12}$$

which consists of the Keplerian energy, the component of the angular momentum in the direction perpendicular to the third body's orbit, and the disturbing function R, which combines both the third-body effect and the nonsphericity perturbation:

$$R = (\omega^2/2)(3x^2 - r^2) - (V + \mu/r) \tag{13}$$

Stability Analysis

When using Hill's problem to investigate the orbital dynamics of low-altitude, planetary satellite orbiters, we found that near-circular orbits suffer from dynamic instability in a wide range of inclinations centered around polar orbits. An analytical study of this problem is presented in Ref. 2, where an approximate, closed-form solution to the orbiter dynamics is obtained for orbits of low eccentricity when considering only the planetary satellite's oblateness. The instability of almost-circular orbits is evidenced by an exponential growth in eccentricity, and this theory predicts unstable orbits for either direct and retrograde inclinations bounded by [Eqs. (43) and (44) of Ref. 2]

$$(1+2\epsilon)/(1+\epsilon) < \tfrac{5}{2}\sin^2 I < (1+2\epsilon)/\epsilon \tag{14}$$

where, for a semimajor axis a and mean motion n, the parameter ϵ, not necessarily small, is

$$\epsilon = J_2[(n/\omega)/(a/\alpha)]^2 \tag{15}$$

where J_2 is the planetary satellite's oblateness coefficient; α is a scaling factor, usually the equatorial radius of the attracting body; and in the first-order approximation a, n are constant for a given orbit.

As shown in Fig. 2, for $\epsilon < 2$ the instability region determined in Eq. (14) encompasses polar orbits, but an additional stability region appears for $\epsilon > 2$. For large values of ϵ, low-eccentricity unstable orbits are confined to a narrow area in the vicinity of the well-known values of the critical inclination in artificial satellite theory.[13]

The dynamics of Eq. (10) is formally equivalent to that produced by the gravity field of a nonsymmetrical rotating body with rotation rate $\boldsymbol{\omega}$. The Lagrangian defining motion is

$$\mathcal{L} = \tfrac{1}{2}\dot{\boldsymbol{r}}\cdot\dot{\boldsymbol{r}} + \boldsymbol{\omega}\cdot\boldsymbol{r}\times\dot{\boldsymbol{r}} + W(\boldsymbol{r};\boldsymbol{\omega}) \tag{16}$$

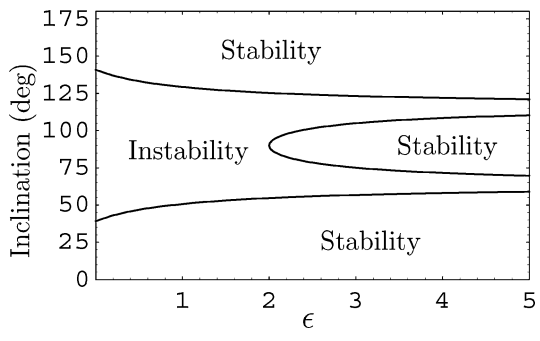

Fig. 2 Regions of stability for different values of ϵ (Ref. 2).

in both cases, but the effective potential function is

$$W = (\omega^2/2)(x^2 + y^2) - V(x, y, z) \tag{17}$$

for the artificial satellite, whereas in the Jupiter–Europa system

$$\begin{aligned} W &= (\omega^2/2)(x^2 + y^2) - [(\omega^2/2)(r^2 - 3x^2) + V(x, y, z)] \\ &= (\omega^2/2)(3x^2 - z^2) - V(x, y, z) \end{aligned} \tag{18}$$

Therefore, instead of using averaging assumptions, we work directly with the equations of motion (10), and proceed as in Refs. 5 and 6 where numerically determined periodic orbits are used to explore stability of motion over three-dimensional space around nonsymmetrical rotating bodies. As Poincaré notes,[7] periodic solutions can help to penetrate nonintegrable dynamical systems: Once a periodic orbit is computed, the stability of that orbit can also be computed, gaining insight in the character of the phase space in the vicinity of the periodic orbit.

To compare our results with those of Ref. 2, we only consider the effect of the oblateness (J_2) coefficient on the potential V:

$$V = -(\mu/r)\left\{1 + J_2(\alpha^2/r^2)\left[\tfrac{1}{2} - \tfrac{3}{2}(z^2/r^2)\right]\right\} \tag{19}$$

where $\mu = 3.201 \times 10^3\ \mathrm{km}^3/\mathrm{s}^2$, the gravitational parameter of Europa; $\alpha = 1565$ km is its equatorial radius; and $(J_2\alpha^2) = 1051.315\ \mathrm{km}^2$. The rotation rate of Europa is $\omega = 2.05 \times 10^{-5}$ rad/s. The numerical values were taken from Ref. 2.

The linear stability of a periodic orbit is determined from the eigenvalues of the monodromy matrix. Because we are dealing with a Hamiltonian problem, eigenvalues appear in reciprocal pairs $(\lambda_i, 1/\lambda_i)$, and as a consequence of the Jacobi integral, Eq. (11), we have one trivial eigenvalue $\lambda_0 = 1$ with multiplicity 2. Then, for periodic orbits of Hamiltonian systems with three degrees of freedom, there are four nontrivial eigenvalues, and two stability indices are normally used[14]:

$$b_i = \lambda_i + 1/\lambda_i, \qquad i = 1, 2 \tag{20}$$

The condition b_i real and $|b_i| < 2$ $(i = 1, 2)$ applies for linear stability.

One of the indices, say b_1, is related to intrinsic, isoenergetic displacements of the orbit in the direction defined by the orbit curvature (normal direction), and in the case of planar motion, it measures the in-plane or horizontal stability ($b_1 \equiv b_h$). The other index, say b_2, is related to intrinsic, isoenergetic displacements of the orbit in the direction defined by the orbit torsion (binormal direction), and in the case of planar motion, it shows the "vertical" stability character ($b_2 \equiv b_v$) of the periodic orbit,[9] which is the behavior of the orbit resulting from perturbations in the out-of-plane direction. The critical value ± 2 for any of the stability indices means that a new family of periodic orbits has likely bifurcated from the original one. When the index taking the value ± 2 is the vertical one, the bifurcating family continues in the direction orthogonal to the plane; on the contrary, $|b_h| = 2$ means that the new family appears on the plane.

Once a periodic orbit is known, we can compute a family of periodic orbits by analytical continuation for variations of a parameter or an integral.[15] The initial periodic orbit we need is computed from the Keplerian approximation that produces almost periodic motion far away from the origin. Then the use of differential corrections provides a true periodic solution of Eq. (10). The tool used for the computation of the families is a vectorial, differential, intrinsic, predictor–corrector algorithm[16] that follows the scheme proposed Ref. 17. Because both the predictor and the corrector stages require the computation of the state-transition matrix, the orbital stability is obtained as a byproduct.

We start from an almost-circular, retrograde, equatorial orbit that is simple-periodic in the rotating frame. Then the natural family of almost-circular, equatorial, simple-periodic orbits is computed for variations of the Jacobian constant.

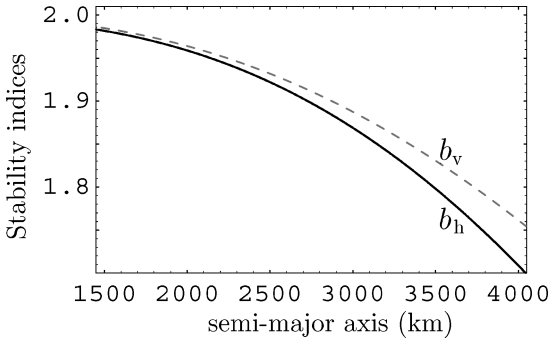

Fig. 3 Stability diagram for the family of equatorial, retrograde orbits.

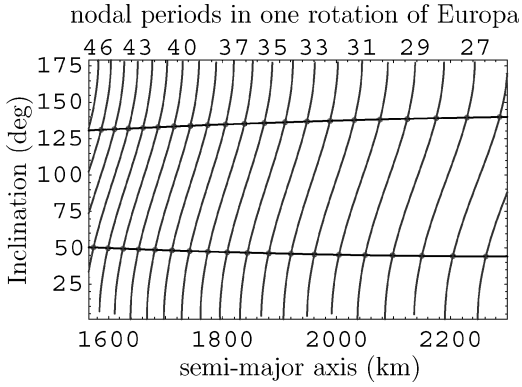

Fig. 4 Families of almost-circular periodic orbits.

In this way, we compute the family of equatorial, retrograde orbits presented in Fig. 3, where the horizontal b_h (solid line) and vertical b_v (dashed line) stability indices are plotted vs the (average) semimajor axis and show stability for all the computed orbits.

Although we do not find critical points in the stability diagram of Fig. 3, we know that there are problems where families of simple-periodic solutions do not show any bifurcation but for some multiplicity indeed they do.[18] We know that horizontal and vertical bifurcations can occur as a consequence of resonances of the satellite's rotation rate with the mean motion of equatorial orbits. Therefore, we search for these resonances, proceeding as in Refs. 5 and 6, and find the corresponding branch families that bifurcate at critical points of multiple-period periodic orbits.

For the Jupiter–Europa system, the typical behavior of the branch families of almost-circular, three-dimensional orbits that are periodic in the rotating frame is presented in Fig. 4, where the families of orbits that are periodic after, from the left to the right, 46, 45, 44, ..., 25 nodal periods are projected as lines onto the a–I plane. Starting from stable, retrograde motion ($I = 180$ deg), variations of the Jacobian constant produce variations on the orbital inclination. At a certain point, corresponding to an inclination between 140 and 135 deg for the computed families, the stability character of the almost-circular orbits changes to instability. The orbits exhibit instability until a certain direct inclination, between 45 and 50 deg for the computed families, where they change again to stability, and the family continues with stable orbits until ending on a planar, equatorial, direct, periodic orbit. Thus, for orbits close to the planetary satellite there is a large interval of inclinations (between 85 and 95 deg wide) centered on 92.5 deg where almost-circular periodic orbits are unstable. In Fig. 4 the region of instability is bounded by the two almost-horizontal lines. Note also in Fig. 4 the decrease in semimajor axes with inclination of the periodic orbits, a known effect for repeating ground track orbits around oblate bodies.[19]

Figure 5 presents the evolution of the stability indices of several of the previous families: from top to bottom, curves represent the evolution of the b_1 index of families of three-dimensional orbits that are periodic after 25, 28, 31, 33, 35, 38, 41, and 44 nodal periods. The horizontal line corresponds to the 8 indices b_2. Although inclination

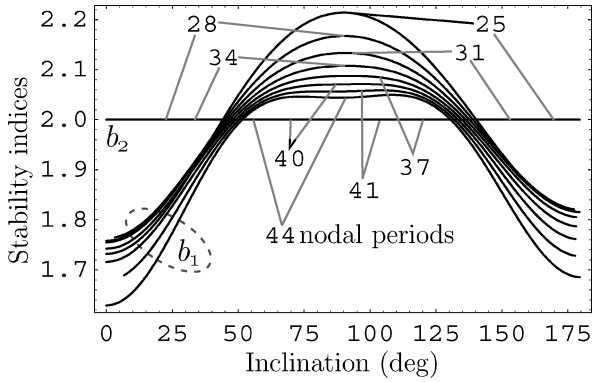

Fig. 5 Evolution of the stability indices b_1, b_2; note that $b_2 = 2$ in all eight cases.

is not the parameter generator of the families, we consider this representation more illustrative because, as previously mentioned, the main effect produced by variations of the Jacobian constant is the variation in the inclination of low-eccentricity orbits. Note in Fig. 5 that, for each family, while one of the stability indices always takes the critical value $b_2 = +2$, the other index crosses the critical line $b_1 = +2$ twice, at different inclinations depending on the computed family.

The index b_2 is the one that coincides with the vertical stability index b_v at the vertical bifurcation, and the fact that $b_2(I) = 2$, $\forall I \in [0, 180\,\text{deg}]$ implies that the family members are always degenerate, and that there is no unique solution for the continuation of the family. Thus, for instance, starting for a periodic orbit with a Jacobian constant $\Gamma = \Gamma_0$ we can propagate the family for increasing values of the Jacobian constant up to a certain orbit with $\Gamma = \Gamma_1$. If the propagation is then carried out for decreasing values of Γ until $\Gamma = \Gamma_0$, we do not necessarily achieve the original solution.

For any ratio ω/n between the planetary satellite's rotation rate and the mean motion of the equatorial orbit, and for a given value of the Jacobian constant, a variety of solutions exists (with both the same period and stability indices) that can be obtained approximately by shifting the initial conditions along the equatorial plane. The dynamic origin of this degeneracy is not evident, and this behavior, previously noticed in similar problems,[5,6] deserves further study. Figure 6 illustrates this behavior for the family of orbits that are periodic after 22 nodal periods. Starting for the full-line orbit, with semimajor axis $a = 2448.25$ km and inclination $I = 20.1$ deg, we can propagate the family for steps $\Delta\Gamma = 3 \times 10^{-4}$ of the Jacobian constant until we obtain a polar orbit. Then the step size can be reversed to $\Delta\Gamma = -3 \times 10^{-4}$ and, after propagating the family for exactly the same number of steps, the dashed-line orbit is obtained, with identical averaged orbital elements except for the argument of the node. Despite the fact that both orbits are different, they have exactly the same period and stability indices.

The degeneracy in the argument of the node admits a geometrical explanation: the unit eigenvalues of the case $b_2 = 2$ imply periodic variations in the binormal direction and make the argument of the node irrelevant. On the other side, the main effect on the orbital elements produced by the instability of the periodic orbits can be clearly appreciated from the geometrical meaning of b_1, an index that is related to intrinsic displacements in the normal direction of the orbit. The exponential growth of the normal displacements produced by the eigenvalues that make $|b_1| > 2$ results in a corresponding exponential growth in eccentricity. But the semimajor axis is not affected because the problem is conservative and we are dealing with isoenergetic displacements.

Elliptic Orbits

In the case of Europa, low-eccentricity periodic orbits are unstable for inclinations that depart more than ~45 deg away from the equatorial plane, both for direct and retrograde motion. For the dynamic model, instability is produced by a bifurcation in phase space where the almost-circular periodic orbits become unstable and two

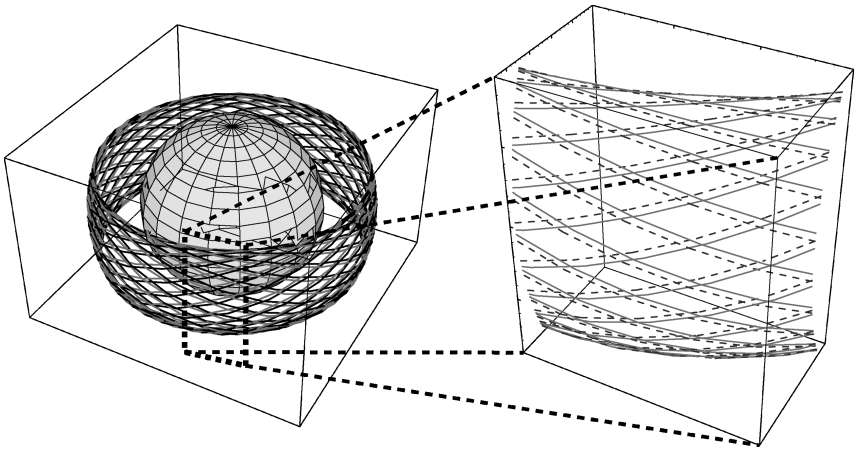

Fig. 6 Two periodic orbits after 22 nodal periods, with different argument of the node.

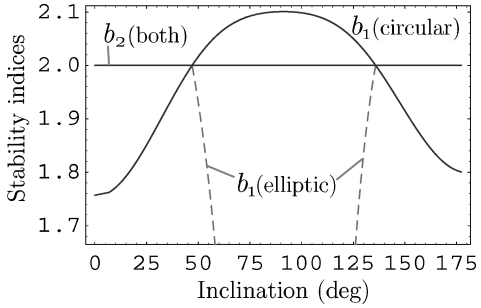

Fig. 7 Stability of the periodic orbits after 35 nodal periods.

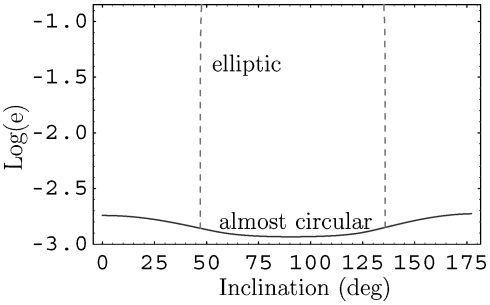

Fig. 8 Eccentricity of the periodic orbits after 35 nodal periods.

new families of stable elliptic orbits, with argument of pericenter at 90 and 270 deg, bifurcate from almost-circular orbits.

As an example, we compute the branch families of elliptic orbits that bifurcate from the family of three-dimensional, almost-circular orbits that are periodic after 35 nodal periods. Figure 7 presents the evolution of the stability indices of these families. Solid lines correspond to the family of almost-circular orbits, and dashed ones represent the families of stable, elliptic orbits, both direct and retrograde, that bifurcate at $I \approx 45$ deg and $I \approx 135$ deg, where $b_1 = b_2 = +2$ and the stability character of almost-circular orbits changes to instability. Figure 8 presents the evolution of the decimal logarithm of eccentricity vs inclination. Elliptic orbits became collision orbits for eccentricities $e \geq 0.166$ for retrograde orbits, and $e \geq 0.134$ for direct orbits; the different values are a consequence of the decrease in the semimajor axes with inclination. Collisions occur in both cases very close to the bifurcation values. The region where noncollision elliptic orbits exist is extremely narrow and ranges from 47.0 to 47.6 deg for direct orbits, and from 134.9 to 135.8 deg for retrograde orbits.

Figure 9 presents three stable solutions that are periodic after 35 nodal periods. The left and right-hand plots are grazing orbits, orbits whose pericenter is very close to the surface of the central body, with an average eccentricity $e = 0.16$, and average inclination $I = 135$ deg. The argument of the pericenter of the elliptic orbits is fixed on average at $g = 270$ deg (left-hand plot) and $g = 90$ deg (right-hand plot), and the orbiter altitude ranges between 6 km over the surface of Europa at the pericenter, and 619 km at the apocenter. The center plot of Fig. 9 shows an almost-circular solution that remains at an altitude of 300 km over the surface of Europa with an average inclination $I = 136$ deg.

Note that the stable, elliptic solutions that exist in the instability region for almost-circular orbits were not predicted in Ref. 2, because the first-order analysis carried out was constrained to low-eccentricity solutions. But due to the rapid growth of the eccentricities in these new solutions with inclination, as shown in Fig. 8, the existence of elliptic orbits does not change the inclination limit for stability.

Qualitative Dynamics

Perturbing function (13) in orbital elements is

$$R = (\omega^2 r^2/2)\{3[\cos(\Omega - \omega t)\cos(g + f) - \sin(\Omega - \omega t)\sin(g + f)\cos I]^2 - 1\} + \tfrac{1}{4}(\mu/r)(\alpha^2/r^2) \times J_2[2 - 3\sin^2 I + 3\sin^2 I \cos 2(g + f)] \tag{21}$$

where f is the true anomaly. All of the periodic terms can be eliminated after a double averaging:

$$\langle R \rangle = \frac{1}{(2\pi)^2}\int_0^{2\pi}\int_0^{2\pi} R\,\mathrm{d}(\omega t)\,\mathrm{d}(nt) = \frac{\omega^2 a^2}{16}\left[(2 + 3e^2)(2 - 3\sin^2 I) + 15e^2 \sin^2 I \cos 2g + 4\epsilon\,\frac{2 - 3\sin^2 I}{(1 - e^2)^{\frac{3}{2}}}\right] \tag{22}$$

and then the qualitative dynamics of the system can be described in terms of the secular variation of the orbital elements using the Lagrange planetary equations. Proceeding as in Ref. 10, we find that besides the trivial integral a there are two more integrals that, regardless of the motion of the nodes, reduce the system to one degree of freedom. One integral is the z component of the angular momentum:

$$\mathcal{G}_z = \sqrt{\mu\, a\,(1 - e^2)}\cos I \tag{23}$$

The other integral is the Jacobi integral of the double-averaged problem:

$$\langle \mathcal{J} \rangle = -\mu/(2a) - \omega\,\mathcal{G}_z - \langle R \rangle \tag{24}$$

Obviously, $\langle R \rangle$ must also be constant. Following Ref. 10, we prefer to use the new integrals

$$C_1 = \frac{\mathcal{G}_z^2}{(\mu\, a)} = (1 - e^2)\cos^2 I \tag{25}$$

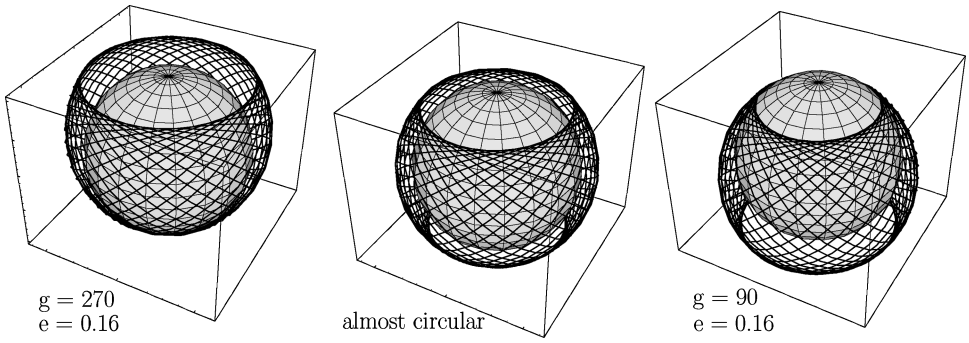

Fig. 9 Stable periodic orbits after 35 nodal periods ($I = 135$ deg).

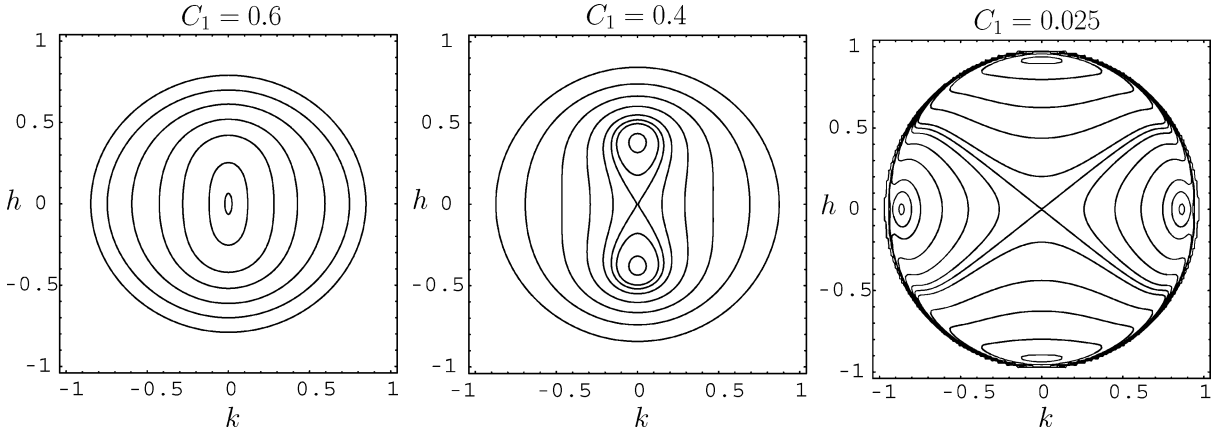

Fig. 10 Contour plots of the averaged problem for $a = 2290$ km.

$$C_2 = \frac{1}{15}\left(\frac{8}{\omega^2 a^2}\langle R\rangle - 3C_1 + 1\right) = e^2\left(\frac{2}{5} - \sin^2 I \sin^2 g\right) + \gamma\frac{2 - 3\sin^2 I}{a^5(1-e^2)^{\frac{3}{2}}} \tag{26}$$

where

$$\gamma = (2/15)\epsilon a^5 = (2/15)\mu J_2 \alpha^2/\omega^2 \tag{27}$$

and in the case of Europa this parameter takes the value $\gamma \approx 0.1$ when the unit of length is Europa's equatorial radius.

Then, without integrating the equations of motion, we can eliminate the inclination between Eqs. (25) and (26) and use contour plots to display the solutions on the e–g plane. The interested reader is addressed to Ref. 10 for details.

The typical dynamic evolution is illustrated with the sequence presented in Fig. 10. Each plot corresponds to a particular point of the a–C_1 parameters plane and provides contour plots in equinoctial coordinates: $k = e\cos g$, $h = e\sin g$. In this kind of projection, contours correspond to different values of C_2, and fixed points are equilibria of the averaged problem. The central point ($k = h = 0$) corresponds to circular orbits while other points are elliptic solutions. The semimajor axis is $a = 2290$ km in all the plots.

Thus, in the left-hand plot of Fig. 10 ($C_1 = 0.6$), the circular orbits are stable because they are surrounded by small ellipses, which means that small perturbations produce a small increase in eccentricity. The center plot ($C_1 = 0.4$) shows that circular orbits are unstable—in the sense that small perturbations of the solution result in a fast growth of eccentricity—and two stable elliptic solutions exist with fixed argument of the pericenter either at $g = 90$ or 270 deg. Note that this behavior is in complete agreement with the stability properties of the periodic orbits computed earlier, where periodic orbit families correspond to fixed points in the (k, h) diagrams.

Up to here the behavior is analogous to Hill's problem studied in Ref. 10. But smaller values of C_1 show that the oblateness perturbation introduces major changes and produces new bifurcations of stable and unstable, highly eccentric orbits with fixed pericenter at $g = 0$ and 180 deg. This is illustrated in the right-hand plot of Fig. 10 ($C_1 = 0.025$). As expected, the new solutions also correspond to periodic orbits. Figure 11 presents a sample stable orbit with fixed pericenter at 180 deg that is periodic after 25 nodal days ($a = 2290$ km, $e = 0.82$, $I = 90$ deg). All the orbits of this family are collision orbits.

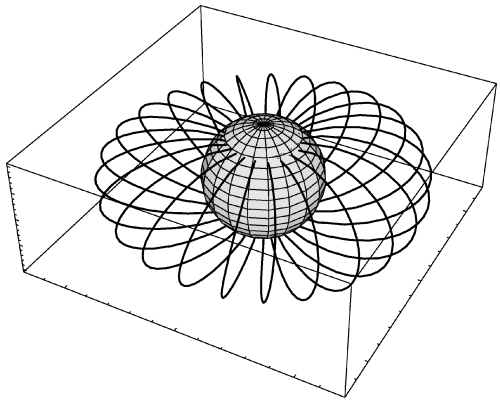

Fig. 11 Polar, collision, periodic orbit after 25 nodal days, with fixed pericenter at 180 deg.

Variations of J_2

To check the influence of the satellite's oblateness for systems of similar characteristics, we compute several families of periodic orbits for variations of the oblateness coefficient. Starting from the Europa case, with an oblateness coefficient $J_2 \approx 4.3 \times 10^{-4}$, we compute the families of orbits that are periodic after 31 nodal periods for variations of J_2, starting from different inclinations. Figure 12 presents several of these new families, made of periodic orbits with direct inclinations, as projected on the J_2–I plane. These families show a consistent behavior, with orbits of increasing inclination for higher values of J_2. The stability character of the periodic orbits varies with J_2 and eventually changes. The periodic orbits where

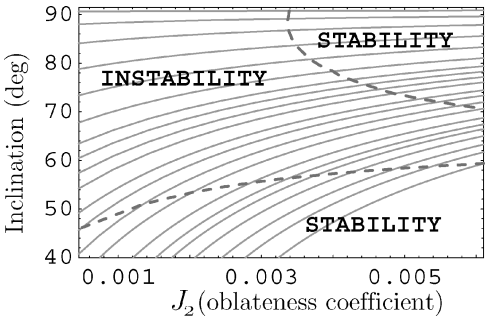

Fig. 12 Variations of J_2; families of periodic orbits (solid lines) after 31 nodal periods.

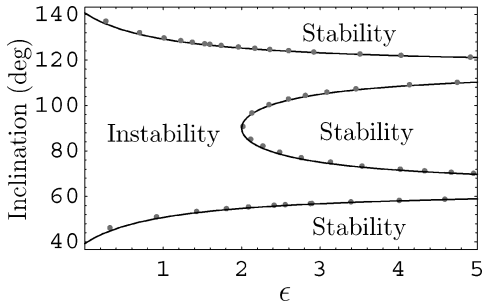

Fig. 13 Stability regions: analytic (solid lines) vs numeric results (dots).

stability changes define the dashed lines of Fig. 12. Then it is possible to determine regions of stability in the J_2–I parametric plane.

As predicted in Ref. 2, the main effect produced by larger values of the oblateness coefficient is a reduction of the instability area. There is a critical value of the oblateness coefficient for which polar orbits become stable and the instability area splits into two narrow areas of unstable motion.

To compare our results with those of Ref. 2, we will now represent the previous computations on the ϵ–I plane, where ϵ is computed from Eq. (15). To do this, for every periodic orbit with a critical stability index we need to compute the values

$$\langle a\rangle = \frac{1}{T}\int_0^T a(t)\,\mathrm{d}t, \qquad n = \frac{2\pi}{T} \tag{28}$$

where $\langle a\rangle$ is the average semimajor axis, n is the mean motion, and T is the nodal period. Figure 13 combines the analytical results of Ref. 2 with the numerical results of this paper. Dots represent the numeric change in stability of the periodic orbits for different values of ϵ, whereas solid lines correspond to Eq. (14). The results of this paper are in general agreement with those of Ref. 2, at least for the case of periodic orbits after 31 nodal periods, but with a slight shift of numeric values to higher inclinations. This shift was already noticed in Ref. 2 when comparing their analytical results to those obtained using numerical integrations of a real model (see Fig. 4 of Ref. 2).

Conclusions

The dynamics of an orbiter under the influence of a planetary satellite undergoes radical changes at certain critical inclination where families of elliptic orbits bifurcate from almost-circular periodic orbits. The values of this critical inclination depend on the planetary satellite's oblateness. With respect to the stability properties of three-dimensional motion close to planetary satellites, the numerical results of this paper confirm previous analytical results of other authors. Thus, both theories are mutually validated by the fact that both analytical and numerical results agree.

Regardless of the motion of the nodes, the averaged problem is integrable, and its representation in equinoctial variables provides a complete insight into the dynamic evolution of the system. The equilibrium solutions of the averaged problem are identified as periodic solutions of the full (nonaveraged) problem.

The time to impact of unstable orbits, an important parameter to design control operations in real missions, cannot be predicted with our theory. But the fact that periodic solutions of Hill's model do exist should make them preferable when maximizing time between control operations.

Future research will include the development of a closed-form analytical theory for the motion of an orbiter around an oblate planetary satellite. After the reduction of the number of degrees of freedom through perturbation methods, we expect to provide a complete description of the dynamics by painting the reduced Hamiltonian. This work is in progress and results will be reported soon.

Acknowledgments

This work has been supported by the Spanish Ministry of Technology and Science (Projects ESP2002-02329, BFM2002-03157, and BFM2003-02137).

References

[1]Space Studies Board, National Research Council, National Academy of Sciences, *New Frontiers in the Solar System: An Integrated Exploration Strategy*, National Academies Press, Washington, DC, 2003, p. 4.

[2]Scheeres, D. J., Guman, M. D., and Villac, B. F., "Stability Analysis of Planetary Satellite Orbiters: Application to the Europa Orbiter," *Journal of Guidance, Control, and Dynamics*, Vol. 24, No. 4, 2001, pp. 778–787.

[3]Johannesen, J. R., and D'Amario, L. A., "Europa Orbiter Mission Trajectory Design," *Advances in the Astronautical Sciences*, Vol. 103, 1999, pp. 895–908.

[4]Hill, G. W., "Researches in the Lunar Theory," *American Journal of Mathematics*, Vol. 1, No. 1, 1878, pp. 129–147.

[5]Lara, M., "Repeat Ground Track Orbits of the Earth Tesseral Problem as Bifurcations of the Equatorial Family of Periodic Orbits," *Celestial Mechanics and Dynamical Astronomy*, Vol. 86, No. 2, 2003, pp. 143–162.

[6]Lara, M., and Scheeres, D. J., "Stability Bounds for Three-Dimensional Motion Close to Asteroids," *Journal of Astronautical Sciences*, Vol. 50, No. 4, 2002, pp. 389–409.

[7]Poincaré, H., *Les Méthodes Nouvelles de la Mécanique Celeste*, Vol. 1, Gauthier-Villars, Paris, 1892, p. 82.

[8]Scheeres, D. J., Williams, B. G., and Miller, J. K., "Evaluation of the Dynamic Environment of an Asteroid: Applications to 433 Eros," *Journal of Guidance, Control, and Dynamics*, Vol. 23, No. 3, 2000, pp. 466–475.

[9]Hénon, M., "Vertical Stability of Periodic Orbits in the Restricted Problem. I. Equal Masses," *Astronomy and Astrophysics*, Vol. 28, No. 3, 1973, pp. 415–426.

[10]Broucke, R. A., "Long-Term Third Body Effects via Double Averaging," *Journal of Guidance, Control, and Dynamics*, Vol. 24, No. 1, 2003, pp. 27–32.

[11]Szebehely, V., *Theory of Orbits*, Academic Press, New York, 1967, pp. 602–611.

[12]Boccaletti, D., and Pucacco, G., *Theory of Orbits*, Astronomy and Astrophysics Library, Vol. 1, Springer-Verlag, Berlin, 1996, pp. 293, 294.

[13]Coffey, S., Deprit, A., and Miller, B., "The Critical Inclination in Artificial Satellite Theory," *Celestial Mechanics*, Vol. 39, No. 4, 1986, pp. 365–406.

[14]Broucke, R., "Stability of Periodic Orbits in the Elliptic Restricted Three-Body Problem," *AIAA Journal*, Vol. 7, No. 6, 1969, pp. 1003–1009.

[15]Siegel, C. L., and Moser, J. K., *Lectures on Celestial Mechanics*, Springer-Verlag, Berlin, 1971, p. 143 ff.

[16]Lara, M., and Peláez, J., "On the Numerical Continuation of Periodic Orbits. An Intrinsic, 3-Dimensional, Differential, Predictor-Corrector Algorithm," *Astronomy and Astrophysics*, Vol. 389, No. 2, 2002, pp. 692–701.

[17]Deprit, A., "Intrinsic Variational Equations in Three Dimensions," *Celestial Mechanics*, Vol. 24, No. 2, 1981, pp. 185–193.

[18]Ollé, M., and Pacha, J. R., "The 3D Elliptic Restricted Three-Body Problem: Periodic Orbits Which Bifurcate from Limiting Restricted Problems. Complex Instability," *Astronomy and Astrophysics*, Vol. 351, No. 3, 1999, pp. 1149–1164.

[19]Cutting, E., Born, G. H., and Frautnick, J. C., "Orbit Analysis for SEASAT-A," *Journal of Astronautical Sciences*, Vol. 26, Oct./Dec. 1978, pp. 315–342.